Chemical Data Collections 31 (2021) 100640

Contents lists available at ScienceDirect

Chemical Data Collections

journal homepage: www.elsevier.com/locate/cdc

Data Article

Investigation on nonlinear optical and antibacterial properties of organic single crystal: p-Toluidinium L-Tartrate

S. Sakthy Priya[a], K. Balakrishnan[a], P. Surendran[a], A. Lakshmanan[a], S. Pushpalatha[a], P. Rameshkumar[a,*], P. Geetha[b], Karthik Kannan[c], Tejaswi Ashok Hegde[d], G. Vinitha[d]

[a] PG and Research Department of Physics, Periyar E.V.R. College (Autonomous), Tiruchirappalli 620 023, Tamilnadu, India
[b] Department of Physics, Quaid-E-Millath Government College for Women (Autonomous),Chennai 600002, Tamilnadu, India
[c] Center for Advanced Materials, Qatar University, PO Box 2713, Doha, Qatar
[d] Division of Physics, School of Advanced Sciences, Vellore Institute of Technology, Chennai 600 127, Tamilnadu, India

ARTICLE INFO

Article history:
Received 22 June 2020
Revised 4 December 2020
Accepted 28 December 2020
Available online 29 December 2020

Keywords:
PTLT crystal
Optical studies
Dielectric studies
Mechanical studies
Z-scan analysis
Antibacterial activity

ABSTRACT

Single crystal of p-Toluidinium L-Tartrate (PTLT) was harvested via slow solvent evaporation technique. The grown PTLT crystal has a *triclinic* structure, *P1* space group. Functional groups were affirmed by FT-IR spectroscopy. The absorption coefficient (α), energy bandgap, and linear refractive index (n_0) were estimated from the UV-Vis-NIR spectrum. A broad emission band observed at 350 nm in the luminescence spectrum of PTLT, corresponds to violet light emission. The dielectric constant and loss were determined by varying the frequency and temperature. The mechanical parameters were determined by the micro-indentation test for various loads. The SHG efficiency of the compound was measured by the powder Kurtz-Perry method. The NLO parameters n_2 (1.731×10^{-9} cm^2W^{-1}), β (0.079×10^{-4} cm W^{-1}), and $\chi^{(3)}$ (9.05×10^{-7} *esu*) were determined by the Z-scan method. In addition, antibacterial activity was carried out against selected foodborne pathogens for pharmaceutical applications .

Specifications table

Subject area	Crystal growth
Compounds	p-Toluidine with L-Tartaric acid
Data category	Spectral
Data acquisition format	XRD, FTIR, UV-Vis-NIR, Luminescence, Dielectric, Micro hardness, SHG, NLO and antibacterial studies
Data Type	Experimental, Analyzed
Procedure	slow solvent evaporation technique

1. Rationale

Crystals are one of the essential key elements of advanced science and technology since they are important for diverse fields including optical modulation, telecommunications, optoelectronics, and optical switching devices, and so on [1–5].

* Corresponding author.
E-mail address: rameshkumarevr@gmail.com (P. Rameshkumar).

https://doi.org/10.1016/j.cdc.2020.100640
2405-8300/

Widespread efforts are being made in recent decades to synthesize and grow high-efficient NLO materials, as it is the elementary key element to be used in the electronics and photonics industries [6,7]. Furthermore, organic compounds have enormous attention in industries due to their cheap-price and elegance in the manufacture of devices. Many organic crystals have superior nonlinear coefficients that can modify and combine into various configurations. Organic materials have higher nonlinearity which is used to produce signal processing devices which include amplitude modulation, harmonic generation, switching, and phase modulation [8–14]. To be used in modern science, the compounds must have higher optical nonlinearity [15–17]. The delocalized conjugated π- electron systems linking the donor (D) and the acceptor (A) offers a variety of exciting chance for developing NLO materials [18]. Organic acid-base crystals were examined for their practical applications in the modern era [19,20]. Organic NLO compound has been used in the integrated hybrid photonic integrated circuitry and are usually flexible because of their intermolecular hydrogen atoms and thus exhibit a high degree of molecular orbitals [21]. Furthermore, the good sensitivity of organic molecules for NLO processes is due to the crystallinity, higher nonlinearity, higher laser damage threshold, inherent synthetic resilience, easy processing, and integration with those of other composites low dielectric constant and losses relative to their inorganic counterparts. Interactions between hydrogen bonds are essential for the design and construction of functional materials [22,23]. Aromatic compounds are useful for NLO applications owing to the delocalized p-electron cloud and the addition of organic acid energy.

In worldwide, foodborne diseases are also the major diseases that affect human health. Many analysts are focused by the researchers to develop some antibacterial agents to treat foodborne diseases. Infectious pathogens like *Staphylococcus aureus, Shigella flexneri, Pseudomonas aeruginosa,* and *Escherichia coli* contaminates the food before or after the preparation which causes illness like pneumonia, urinary tract infections, abscesses, respiratory infections, diarrhoea, and food poisoning. The bacteria release toxins in the food which is very detrimental to human health [24,25]. *Escherichia coli, Shigella flexneri,* and *Staphylococcus aureus* are the major foodborne pathogens that were declared by the National Public Health Institute (CDC, USA) [26]. Therefore to overcome the problem, researchers are giving an effort to replace the existing drugs by with new drugs with enhanced antibacterial activity.

The crystal structures of p-Toluidinium L-Tartrate were already studied by Renuka et al. [27]. Organic crystals are strong prospects for NLO performance than inorganic crystals. This is due to the π conjugated arrangement produced by organic crystals, which allows an electron donor with an acceptor process for electron cloud movement, which leads to nonlinearity. Tartaric acid, with its chiral structure, demonstrated the ability to combine with certain organic bases, which is a critical requirement for the efficiency of the NLO. To reveal their competence in SHG applications a variety of tartrate derivatives were inspected. The Toluidine Tartrate is a hydrogen bonded complex of L-Tartaric acid and p-toluidine. The development of the proton carboxylic donor (COO-) group in tartaric acid and the proton accepter amino (-NH2) group in toluidine provides PTLT crystal as a suitable material for the study of its structure and NLO activity [28–30]. In the present work, few important characterization analyses and detailed discussion of PTLT crystal are reported for the first time through this communication. The grown crystal has potential antibacterial activity compared to some other single-crystal materials [31–40].

To overcome the above problems, in this article, p-Toluidinium L-Tartrate crystal was grown and were investigated towards PXRD, FTIR, UV-Vis-NIR, Luminescence, dielectric, mechanical, SHG efficiency, and third-order nonlinear optical (TONLO) properties of the synthesized organic crystal. In addition, the antimicrobial activities of the prepared single crystal against foodborne pathogens have been examined.

2. Procedure

2.1. Crystal growth

p-Toluidinium L-Tartrate (PTLT) crystal was synthesized using the precursor's in (1:1) ratio of p-Toluidine (C_7H_9N) and L-Tartaric acid ($C_4H_6O_6$) which was dissolved separately in deionized water then it was added together. The prepared solutions were mixed and stirred well for 12 h to attain a homogeneous mixture. Using filter paper (Whatman), the mixture was filtered. Then the filtrate was preserved in a constant temperature bath at 30 °C under controlled evaporation and a pale brown color crystal ($6 \times 5 \times 4$ mm^3) was grown after 35 days as displayed in Fig. 1.

2.2. Characterization of PTLT crystal

In order to find the lattice parameters and crystalline nature of the grown sample, PTLT crystal was finely powdered and subjected to XPERT-PRO X-ray powder diffractometer with CuK_α radiation (~1.5406 Å,0.1 min^{-1}, 10° to 80°). The molecular bonding and functionalgroups found in the PTLT crystal were measured by the KBr pellet approach using Perkin Elmer (Model: spectrum two), FTIR spectrometer recorded at ambient temperature in the wave number range of 4000–400 cm^{-1}. The UV-Vis-NIR absorbance spectrum of the PTLT crystal was obtained at room temperature by using UV-Vis-NIR (Shimadzu/UV 2600) spectrophotometer in the range of 200–1100 nm. The luminescence spectrum of PTLT single crystal was measured by Spectro-fluorophotometer (Shimadzu/RF 6000) with source as Xenon arc lamp. The synthesized PTLT crystal was studied by the SHIMADZU HMV-GT series with a diamond indenter microhardness tester. The dielectric analysis as a function of applied frequency (50 Hz to 200 kHz) was explained by using the LCRZ meter (model: TH2816A). The SHG frequency conversion efficiency of powdered PTLT sample was found using Q-switched Nd-YAG laser (1.23 mK/pulse, 1064 nm) by Kurtz and Perry powder method. The TONLO properties of PTLT crystal was measured by the Z-scan technique.

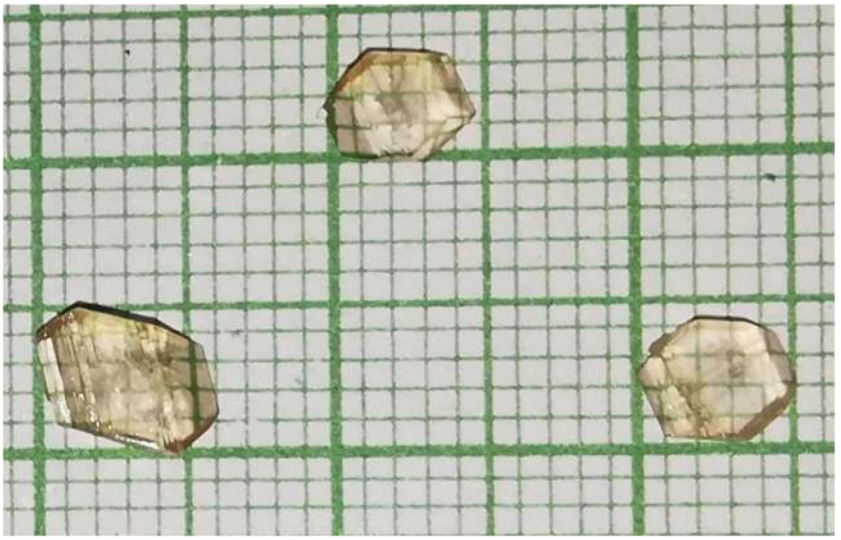

Fig. 1. As grown PTLT single crystal.

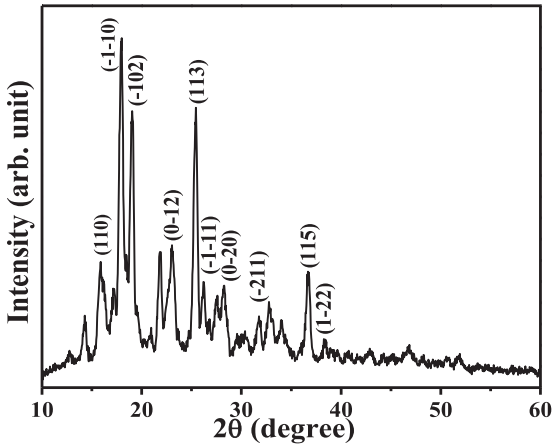

Fig. 2. The XRD pattern of the grown PTLT single crystal.

2.3. Antibacterial studies

Agar well diffusion technique has been used to assess the antimicrobial ability of the p-Toluidinium L-Tartrate (PTLT) compound. The microbes grown in nutrient broth and agar plates were coated with *Bacillus cereus, Staphylococcus aureus* (gram-positive), and *Shigella flexneri, Pseudomonas aeruginosa, Vibrio cholerae, Escherichia coli* (gram-negative) through inoculation loops. First, the stock solution 0.1 g of finely grained powdered PTLT compound was diluted in 1 mL of double distilled water and 0.1 μL of sample solution was poured into the well. Subsequently, the plates were sealed and incubated face even further in an incubator at 37 °C for 24 h, accompanied by measurements of the zone of inhibition (mm).

3. Data, value and validation

3.1. Structural studies

Fig. 2 shows well established Bragg's peaks that affirm the high crystalline nature of the title compound and it is free from structural grain boundaries [41]. The corresponding peaks and planes were indexed using *checkcell* software. The cell parameters values calculated are $a = 5.67$ Å, $b = 6.87$ Å, $c = 13.41$ Å, $\alpha = 88.67°$, $\beta = 81.5°$ $\gamma = 71.35°$ and $V = 489$ Å^3 which superiorly matches with the previously report [28]. It discloses a *triclinic* crystal system and P1 space group. The microstrain present in the lattice were determined by the Hall-Williamson equation as,

$$\beta \cos\theta = \frac{K\lambda}{D} + 4\eta \, Sin\theta \tag{1}$$

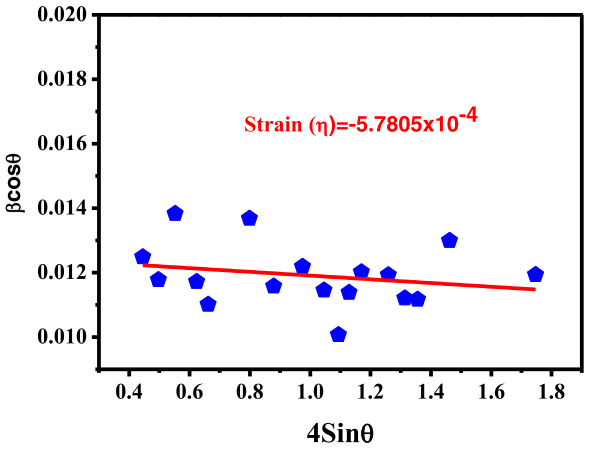

Fig. 3. W-H plot of PTLT crystal.

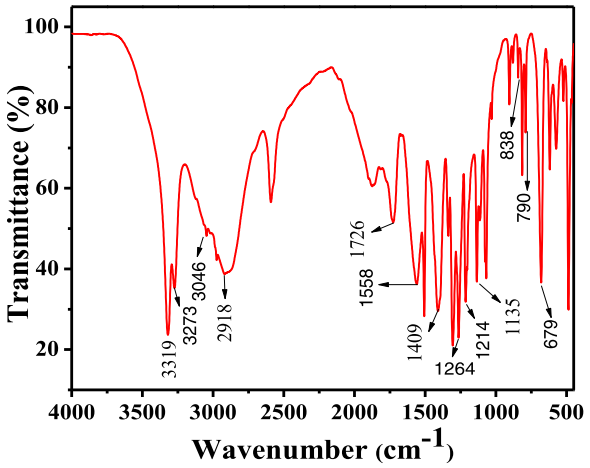

Fig. 4. FTIR spectrum of PTLT crystal.

Where β is diffraction peaks (FWHM), θ is diffraction angle, K is constant, λ is X-ray wavelength and D is the crystalline size (14 nm). The plot of $\beta\cos\theta$ *versus* $\sin\theta$ is given in Fig. 3. The strain value of the PTLT crystal is -5.7805 $\times$ 10^{-4}. The negative strain value represents the compressive strain that is attributed to the crystal lattice defects. The crystal properties are influenced by dislocation density which is evaluated by,

$$\delta = \frac{1}{D^2} \tag{2}$$

The dislocation density value is 5.1020 $\times$ 10^{15} (Lines/m^2).

3.2. Vibrational analysis

The molecular composition of the PTLT sample was affirmed by the FTIR spectrum (Fig. 4). The intense sharp peaks at 3319 cm^{-1} belong to surface hydroxyl group stretching mode. Hydroxyl groups show a crucial part in enhancing the antibacterial activity of PTLT crystal [42,43]. The peaks identified at 3273 and 3046 cm^{-1} are ascribed to asymmetric and symmetric stretching modes of N-H in the amino (NH_3^+) group. The absorption peaks at 2918 and 1409 cm^{-1} are because of the existence of methyl groups affirmed by the symmetric and asymmetric deformation of C-H and the vibration stretching of C=C at 1558 cm^{-1}. The band at 1214 cm^{-1} is associated with C-N stretching. Peaks identified around 1200–1000 cm^{-1} and 1000–700 cm^{-1} are due to the in and out-of-plane bending of the C-H aromatic ring [28]. The occurrence of C=O vibration mode of PTLT is evident at the peak 1726 cm^{-1}. The peak at 1135 cm^{-1} refers to the C-O stretching vibration of L-Tartaric acid.

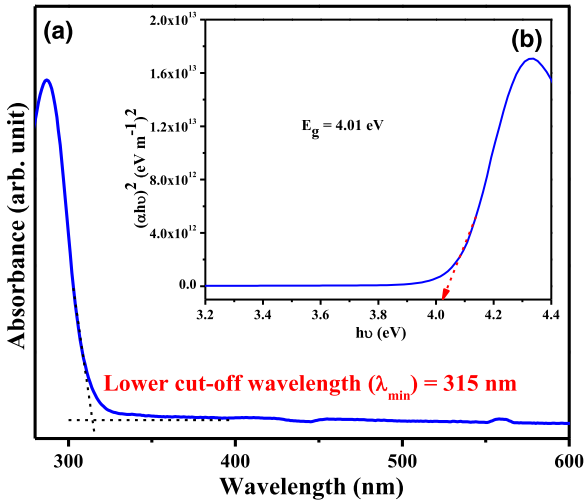

Fig. 5. **(a)** UV-Vis-NIR absorption spectrum (b) Graph of $(\alpha h\upsilon)^2$ *versus* hυ for PTLT crystal.

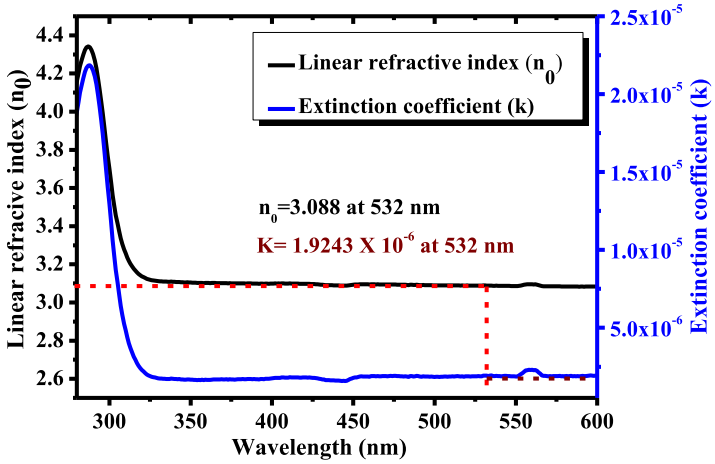

Fig. 6. Wavelength dependence of (a) linear refractive index (n_0), (b) Extinction co-efficient (K).

3.3. Linear optical studies

The PTLT crystal was analyzed to assess the suitability for the optical application using the UV-Vis-NIR spectrum [44]. As shown in Fig. 5(a), the lower cut-off wavelength is found to be at 315 nm that is near the UV region because of the π-π^* transitions. The significant absorption under 350 nm is owed to electronic transitions [45]. Eq. (3) is used to calculate the bandgap as given by,

$$(\alpha h\upsilon) = A(h\upsilon - E_g)^n \tag{3}$$

where A is a constant, E_g is bandgap, h is 6.626 × 10^{-34} Js, and exponent n is subjected to the type of transition in the sample. Energy bandgap (E_g) is analyzed using Tauc's plot by drawing a graph between $(\alpha h\upsilon)^2$ *versus* $h\upsilon$ as displayed in Fig. 5(b). Theoretically, the optical bandgap can be calculated by E_g=1240/λ (eV). The calculated optical energy bandgap value is 3.94 eV which is in superior agreement to the experimentally evaluated bandgap value (4.01 eV). The PTLT crystal has a broad bandgap which can be applicable for optoelectronic devices [46]. The quantity of absorption by the transmission of electromagnetic waves over the medium is explained by extinction co-efficient (K) by using the formula,

$$K = \frac{\alpha\lambda}{4\pi} \tag{4}$$

The disparity of extinction co-efficient *Vs* wavelength is revealed in Fig. 6(a). The calculated extinction coefficient is found to be 1.9243 × 10^{-6} at 532 nm. The reflectance in relation to the absorption co-efficient is derived by the following equation,

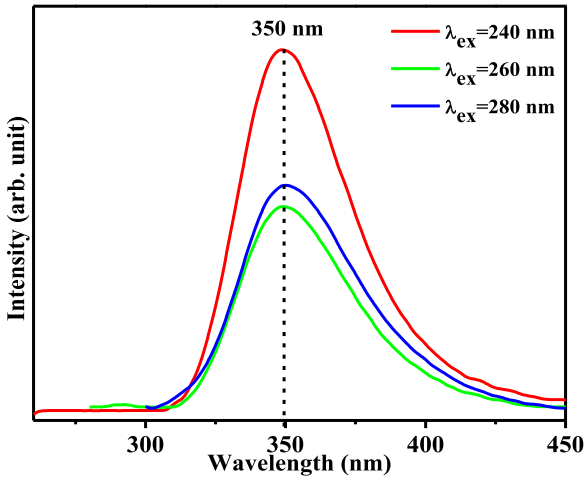

Fig. 7. Luminescence spectra of PTLT crystal at different excitation wavelength.

$$R = \frac{\exp(-\alpha t) \pm \sqrt{\exp(-\alpha t)T - \exp(-3\alpha t)T + \exp(-2\alpha t)T^2}}{\exp(-\alpha t) + \exp(-2\alpha t)\alpha T} \tag{5}$$

Where 'T' is the transmittance, 't' is the size of the crystal (1.15 mm). The refractive index (n_0) of the PTLT crystal in terms of reflectance can be determined by the formula,

$$n_0 = -(R+1) \pm 2\frac{\sqrt{R}}{(R-1)} \tag{6}$$

Fig. 6(b) displays the plot of n_0 *versus* wavelength and n_0 of PTLT crystal is 3.088 at the wavelength of 532 nm which is used to compute TONLO parameters of the compound. From the optical analysis, it enunciates that the PTLT crystal has a strong optical performance for optoelectronic devices.

3.4. Luminescence analysis

For the use of LED applications, luminescence analysis is done for the grown crystal to determine the luminescence property of the sample. The emission peak was recorded at room temperature for three excitation wavelengths of 240, 260, and 280 nm which is presented in Fig. 7, and was noted that the excitation wavelength increases with a decrease in the intensity and there is no peak shift. In this spectrum, incessant emission of light exposure transition of the system on the ground and excited states is attributed to the existence of carbon bonds of π- electron transition [47]. A strong emission peak was found at 350 nm, which could be ascribed to the transition of charge in the amine groups (NH_3^+) of the PTLT crystal. In material research, luminescence studies play a vital role in different fields like electroluminescent display, biomedical fields, photochemistry, chemical sensors and also in chemistry research areas [48]. The grown PTLT crystal emission peak at 350 nm is found in the ultraviolet (UV) region, and is suitable for UV sensors and fluorescence detectors [49].

3.5. Dielectric analysis

The electro-optic features of the sample were studied by the dielectric study. The PTLT crystal was polished and coated with graphite for accuracy in measurements. The prepared sample thickness is 1.3 mm. Dielectric analyses were taken for the alternating electric field with different frequencies from 50 Hz to 200 kHz at various temperatures (30 to 70 °C). The dielectric constant (ε') and loss (ε") of the compound was evaluated using the standard formula [50]. Fig. 8 (a-b) depicts the normal occurrence, that ε' and ε" increases as the decrease in frequency with respect to different temperatures. Electronic, orientation, ionic, and space charge polarization is responsible for the increase in dielectric constant for lower frequency. In the electric loss, the sample is exposed to a varying electric field, where the material loses its energy. Due to the space charge polarization ε" decreases as the frequency increases which confirms that the sample has strong optical consistency with fewer defects [51]. For all temperatures, the ε' and ε" has lesser values at a higher frequency is an optimal phenomenon for electro-optic applications [52]. The AC conductivity can be evaluated by,

$$\sigma_{ac} = 2\pi f \varepsilon' \varepsilon_0 \tan\delta \tag{7}$$

Where f is frequency applied and ε_0 is vacuum permittivity (8.854×10^{-12} F/m). The disparity of AC conductivity with respect to frequency for various temperatures is given in Fig. 9.

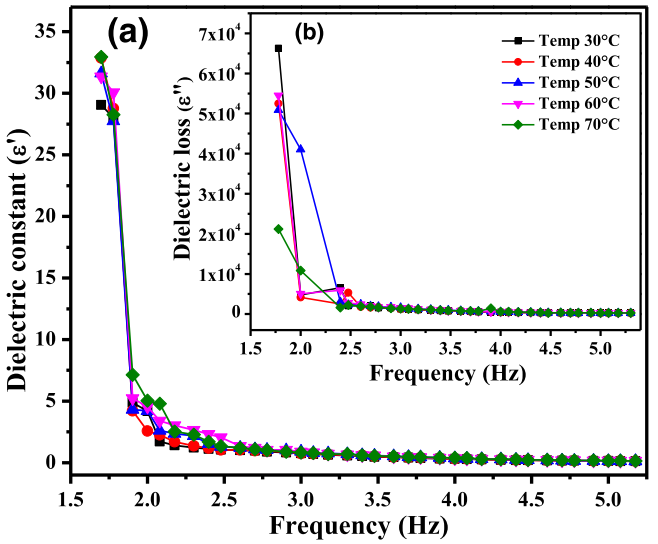

Fig. 8. (a) Dielectric constant and (b) dielectric loss versus frequency for PTLT crystal.

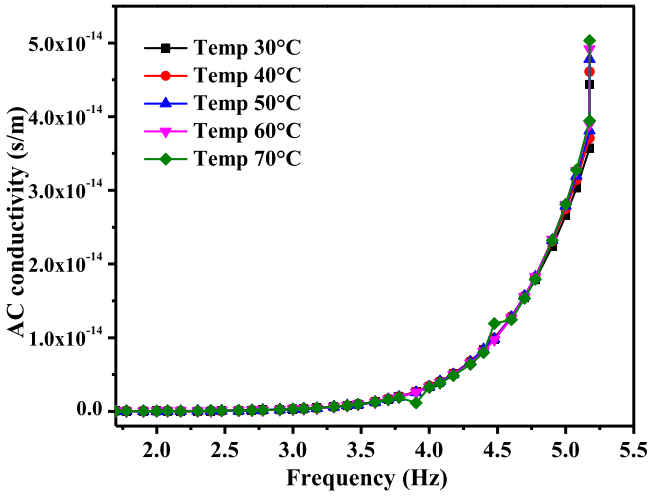

Fig. 9. AC conductivity plot for PTLT crystal.

3.6. Electronic Polarizability (α)

Electronic polarizability is the noteworthy parameter to evaluate the efficiency of the nonlinear materials. Electronic polarizability of the material can be theoretically determined by Penn analysis, Clausius-Mossotti expression, and optical bandgap. The calculation theoretically displays that the dielectric constant could be governed by valence electron plasma energy, Penn gap (E_P), Fermi energy (E_F), and electronic polarizability (α). The density of the PTLT sample is evaluated from the relation,

$$\rho = \frac{MZ}{N_A V} \tag{8}$$

Where M is the molecular mass of the PTLT compound, Z is the unit cell, N_A is the Avogadro number (6.022×10^{23} mol^{-1}) and V is the volume. The valence electron plasma energy ($\hbar\omega_\rho$) can be evaluated by

$$\hbar\omega_\rho = 28.8\sqrt{\frac{(Z \times \rho)}{M}} \tag{9}$$

The valence electron of PTLT sample is $Z = (11 \times 4) + (15 \times 1) + (6 \times 6) + (1 \times 5) = 100$ where ρ is the density, valence electron of C, H, N and O are 4, 1, 5 and 6 respectively. Based on the Penn model, average E_P and E_F is determined

Table 1
Polarizability parameters of the grown PTLT crystal.

Parameters	Values
Molecular weight	257.237 (g/mol)
Density	1.3682 (g/cm^{-3})
Plasma energy	21.0039 (eV)
Penn gap	1.9034 (eV)
Fermi energy	17.0668 (eV)
Penn analysis	7.26 × 10^{-23} (cm^3)
From Clausius–Mossotti equation	7.28 × 10^{-23} (cm^3)
Optical energy band gap	3.7639 × 10^{-23} (cm^3)

using,

$$E_P = \frac{\hbar\omega_\rho}{\sqrt{\varepsilon_r - 1}} \tag{10}$$

$$E_F = 0.2948(\hbar\omega_p)^{4/3} \tag{11}$$

Calculate electronic polarizability (α) of the sample is evaluated by

$$\alpha = \left[\frac{(\hbar\omega_\rho)^2 s_0}{(\hbar\omega_\rho)^2 s_0 + 3E_P^2}\right] \times \frac{M}{\rho} \times 0.369 \times 10^{-24} cm^3 \tag{12}$$

Where, $s_0 = 1 - [\frac{E_P}{4E_F}] + \frac{1}{3} + [\frac{E_P}{4E_F}]^2$

The electronic polarizability (α) is also affirmed and computed using Clausius-Mosotti expression,

$$\alpha = \frac{3M}{4\pi N_A \rho}\left(\frac{\varepsilon_r - 1}{\varepsilon_r + 2}\right) \tag{13}$$

ε_r is the dielectric constant at 200 kHz (room temperature). The electronic polarizability from the energy bandgap can be determined by the following equation,

$$\alpha = \left[1 - \frac{\sqrt{E_g}}{4.06}\right] \times \frac{M}{\rho} \times \ 0.396 \ \times 10^{-24} cm^3 \tag{14}$$

The calculated electronic polarizability values from Penn analysis and Clausius-Mosotti equation are in better agreement with each other. The calculated electronic polarizability values are summarized in Table 1.

3.7. Vickers microhardness test

The Vickers microhardness measurement is done to identify the details regarding the crystal's mechanical strength which is significant for device fabrication. The smooth surface PTLT crystal is taken for the measurement at ambient temperature for different loads from 25 to 100 g with an indentation time of 5 s. Vickers microhardness (Hv) is estimated by

$$H_v = 1.854 \ \times \frac{P}{d^2}\left(kg/mm^2\right) \tag{15}$$

Where P is load (kg), d is diagonal length (mm) and Hv is Vickers microhardness number (Kg/mm^2). As load P is increased, hardness number values also increase as shown in Fig. 10(a) and are related to the reverse indentation effect. Because of the internal pressure, the crystal starts to crack above 100 g during indentation. Meyer's index was evaluated by

$$P = Kd^n \tag{16}$$

$$\log P = \log k + n \ log \ d \tag{17}$$

Where n is Meyer's index and k is material constant. A graph between log P *versus* log d is displayed in Fig. 10(b) and the work hardening coefficient is determined as 3.612. According to Onitsch [53], if n is >1.6, and then the materials refer to a soft category which is convenient for the construction of optoelectronic applications. The yield strength (σ_y) could be determined by using H_v value as Meyer's index were estimated as 2.6 (2<n<3) using the equation,

$$\sigma_y = \frac{H_v}{2.9}\ [1 - (n-2)]\left(\frac{12.5(n-2)}{1-(n-2)}\right)^{n-2} \tag{18}$$

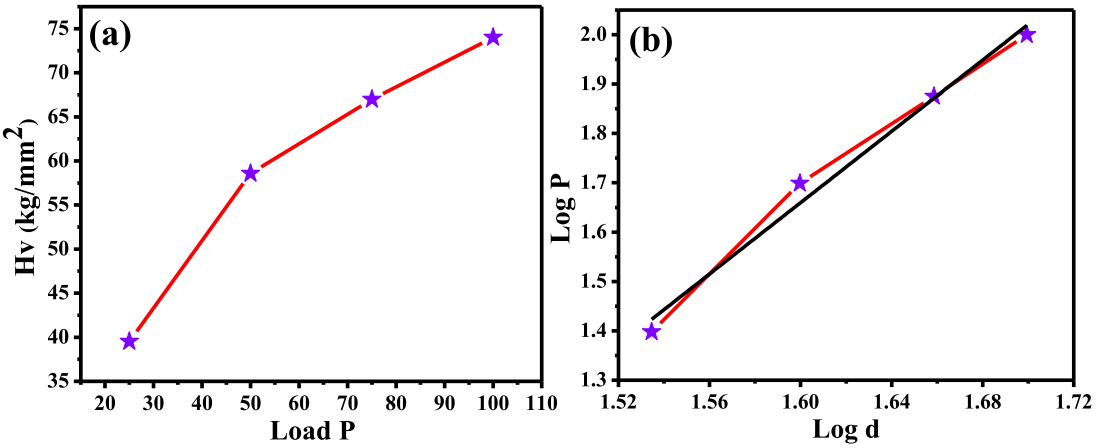

Fig. 10. (a) Variation of Hv vs. load P (g) and (b) log P vs. log d.

Table 2
Calculated mechanical parameters of PTLT crystal.

Load P (g)	H_v (kg/mm^2)	H_K (kg/mm^2)	$C_{11} \times 10^{14}$ (Pa)	$K_c \times 10^4$ (kg/m$^{3/2}$)	B_i (μ/m½)	σy (GN/m^2)
25	39.5292	0.303377	6.11121	9.367228	4.219946	10.2773
50	58.5801	0.449588	12.16419	18.734456	3.126864	15.4095
75	66.9743	0.514011	15.37659	28.101684	2.383284	19.8557
100	74.0192	0.568080	18.3178	37.468912	1.975483	20.6092

A graph of load P *versus* σ_y is seen in Fig. 11(a). Fracture toughness (K_c) of the material is explained by the fracture toughness arises due to the cracks formed during the course of indentation under uniform loading [54].

$$K_c = \frac{P}{\beta_0 C^{3/2}} \tag{19}$$

β_0 is constant and C is the crack length of the crystal. Fig. 11 (b) shows the load (P) *Vs* fracture toughness. Brittleness index (B_i) describes the induced fracture in the crystal without considerable deformation [55] and is calculated by

$$B_i = \frac{H_v}{K_c} \tag{20}$$

The interatomic bonding strength of the crystal is calculated by elastic stiffness constant (C_{11}) by Wooster's empirical equation [56],

$$C_{11} = (H_v)^{7/4} \tag{21}$$

A plot of load P *versus* C_{11} is seen in Fig. 11(c). Knoop hardness of the material can be evaluated following formula,

$$H_k = 14.229\left(\frac{P}{d^2}\right)\ (kg/mm^{-2}) \tag{22}$$

A plot of load (P) *versus* Knoop hardness (H_k) is seen in Fig. 11(d). The calculated mechanical parameters for various loads are tabulated in Table 2.

3.8. SHG studies

The SHG of the PTLT compound was analyzed by the powder Kurtz and Perry method. In the microcapillary tube, the grained sample was filled. The sample was subjected to the laser beam (1064 nm) with a pulse width of 10 ns and with input energy of 1.1 mJ. Green emission light (532 nm) was produced towards the photomultiplier tube which was detected. The presence of delocalized electron and intermolecular interaction in the sample is liable for the nonlinear response of the PTLT crystal [57]. The output value has comparable output with the standard material (KDP). Hence, PTLT crystal is suitable for frequency conversion applications.

3.9. Z-scan analysis

Sheik Bahae et al. [58] introduced the *Z*-Scan method which is the simple, sensitive tool to measure the nonlinearity and the changes in the nonlinear absorption coefficient (β) and refractive index (n_2). In this technique, CW laser (532 nm)

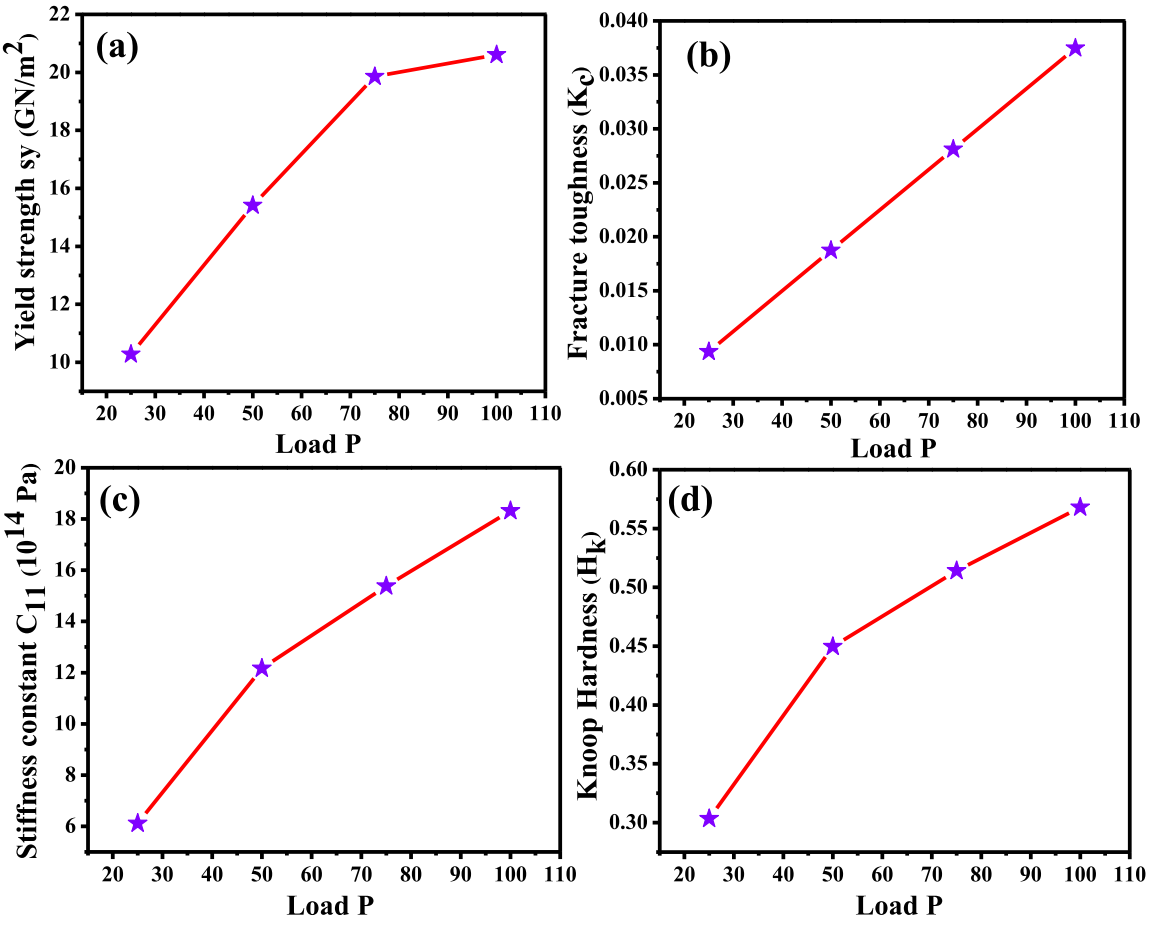

Fig. 11. (a) Yield strength (σy) vs. load P (g), (b) fracture toughness vs. load P (g), (c) stiffness constant (C_{11}) vs. load P (g) and (d) knop hardness vs. load P (g).

was used with a focal length of 130 mm and intensity of the laser 0.01478 (MW/cm^2). The material was placed in the Z-axis along with propagation of laser source and was moved horizontally in the positive (+Z) to negative (-Z) direction. The recorded closed aperture (CA), open aperture (OA) curves, and ratios of CA/OA are revealed in Fig. 12 (a-c). In an open aperture, the minimum transmittance at the focus (Z=0) suggests that reverse saturable absorption (RSA). In closed aperture, it indicates peak followed valley that refers to the self-defocusing nature. Using standard relation, third-order NLO measurements were estimated [59–61]. The actual and imaginary aspects of the TONLO susceptibility ($\chi^{(3)}$) may be determined using the following equation,

$$R_e\left(\chi^{(3)}\right) = \frac{10^{-4}\varepsilon_o c^2 n_o^2 n_2}{\pi}\ \left(\mathrm{cm}^2/\mathrm{W}\right) \tag{23}$$

$$I_m\left(\chi^{(3)}\right) = \frac{10^{-2}\varepsilon_o c^2 n_o^2 \lambda\beta}{4\pi^2}\ \left(\mathrm{cm}^2/\mathrm{W}\right) \tag{24}$$

The TONLO susceptibility ($\chi^{(3)}$) could be determined by the equation,

$$\chi^{(3)} = \sqrt{(R_e\chi^{(3)})^2 + (I_m\chi^{(3)})^2} \tag{25}$$

The calculated TONLO properties for the PTLT sample are n_2 is 1.731 $\times$ 10^{-9} (cm^2/W), β is 0.079 $\times$ 10^{-4} (cm/W), and $\chi^{(3)}$ is 9.05 $\times$ 10^{-7} (*esu*). The calculated NLO parameters are summarized in Table 3. The PTLT sample has higher NLO susceptibility compared with several other reported NLO crystals and is tabulated in Table 4. [19, 62–67]. From the Z-scan analysis, the grown PTLT crystal indicates a negative sign of the n_0 value, which is due to the self-defocusing nature, and the nonlinear absorption is identified as reverse saturable absorption which is a most suitable property for optical switching and optical limiter devices.

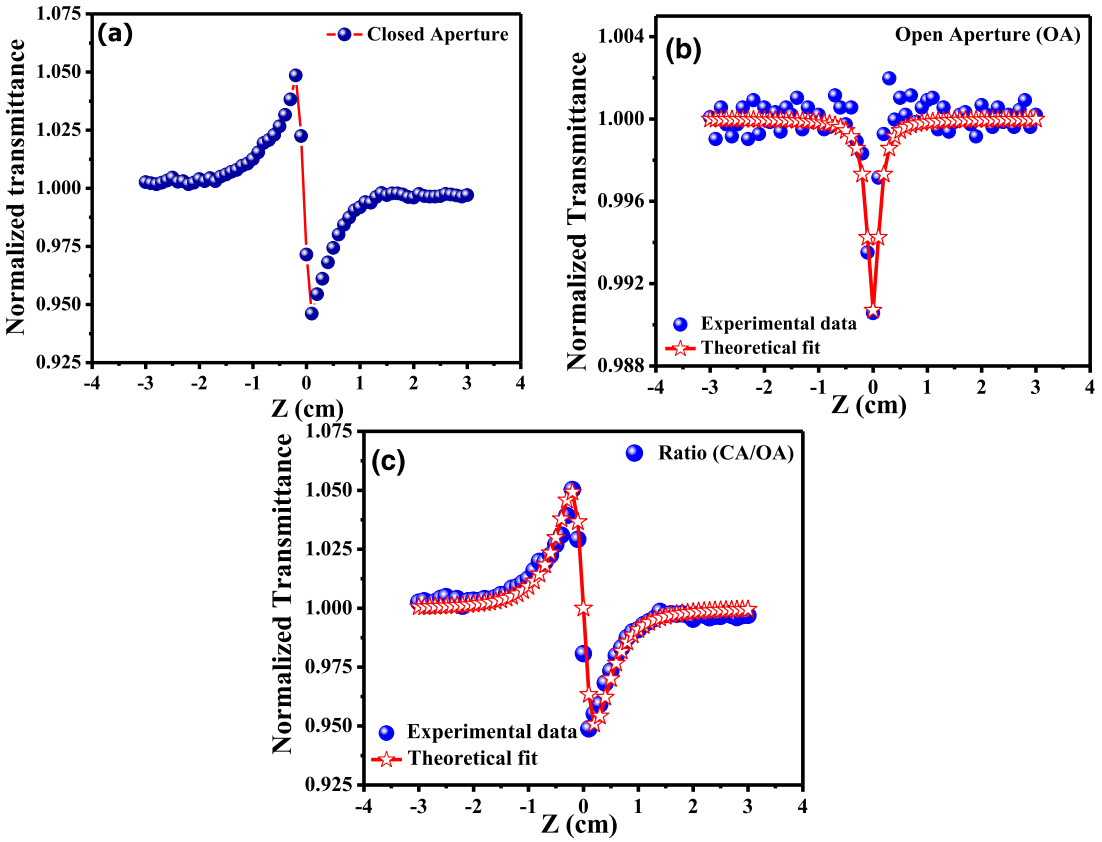

Fig. 12. (a) Closed aperture (b) Open aperture and (c) Ratio (CA/OA) Z-scan curve of PTLT crystal.

Table 3
Third–order (NLO) parameters of the grown PTLT crystal.

Parameters	Values
Laser wavelength	532 (nm)
Focal length of lens used	130 (mm)
Radius of aperture used	1.5 (mm)
Radius of the beam on aperture	3 (mm)
Intensity of the laser at the focus	0.01478 (MW/cm^2)
Reighley range (Z_R)	1.271 (mm)
Nonlinear refractive index (n_2)	1.731×10^{-9} (cm^2/W)
Nonlinear absorption coefficient (β)	0.079×10^{-4} (cm/W)
Real part of third order nonlinear susceptibility (Re $\chi^{(3)}$)	4.1847×10^{-7} (esu)
Imaginary part of third order nonlinear susceptibility (Im $\chi^{(3)}$)	8.0287×10^{-7} (esu)
Third order nonlinear susceptibility ($\chi^{(3)}$)	9.05×10^{-7} (esu)

Table 4
Comparison of third order nonlinear optical susceptibility ($\chi^{(3)}$) values of PTLT with other NLO materials.

Crystal	Third order NLO susceptibility ($\chi^{(3)}$)	Reference
PTLT	**9.05×10^{-7} (esu)**	**Present work**
3-A2CPB	4.82×10^{-07} (esu)	[19]
CT	8.78×10^{-07} (esu)	[52]
TP4N	4.33×10^{-08} (esu)	[53]
AAP	6.20×10^{-09} (esu)	[54]
LTT	7.1368×10^{-10} (esu)	[55]
VMST	9.6963×10^{-12} (esu)	[56]
LTP	5.382×10^{-14} (esu)	[57]

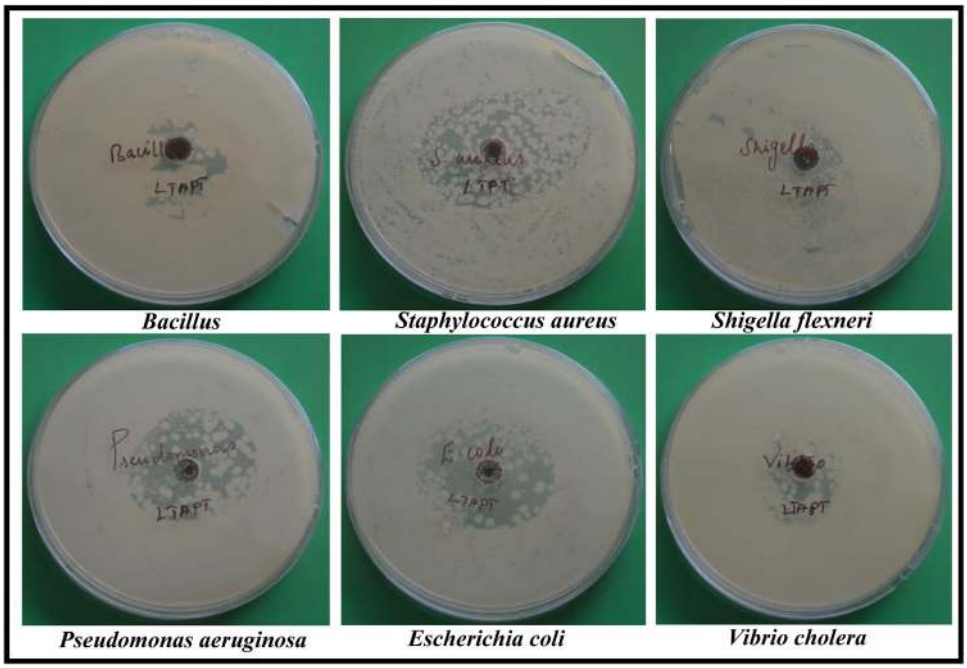

Fig. 13. Photographs of antibacterial plates of the grown PTLT single crystal.

Table 5
Zone of inhibition against particular bacterial (mm).

Tested bacteria	Gram reaction	Zone of inhibition (mm)
Bacillus cereus	+ve	18
Staphylococcus aureus	+ve	40
Shigella flexneri	–ve	24
Pseudomonas aeruginosa	–ve	35
Vibrio cholera	–ve	22
Escherichia coli	–ve	35

3.10. Antibacterial studies

The evaluation of antibacterial activity for the finely grained PTLT compound was carried out against gram +Ve (*S. aureus, B. cereus,*) and gram -Ve (*V. cholerae, S. flexneri, P. aeruginosa, E. coli*) bacterial strains via disk diffusion method. The obtained zone of inhibition plate photos is shown in Fig. 13. If the inhibition zone is larger than 6 mm, then it indicates higher antimicrobial activities [25, 68, 69]. From the results, PTLT has better antibacterial activity against tested bacterial strains. Among six bacteria, *Staphylococcus aureus* is more sensitive to the PTLT crystal. The zone of inhibition (ZOI) of PTLT compound is tabulated in Table 5.

The hydrogen bonding interactions in the title compound greatly enhance the antibacterial efficiency [70]. The present sample can penetrate into the cell membrane, and increase permeability, reduce metabolic activity, and destroy the bacterial cells. The delocalized π-electrons have strengthened lipophilicity, contributing to the degradation of the cell's permeability and thereby retarding normal cell processes [71–73]. Hence the grown PTLT crystal will be a promising candidate for the development of antibiotic drugs against tested bacterial strains. From Table 6, the antibacterial activities of PTLT compound possess good antibacterial activity (ZOI) compared with some other reported organic and inorganic materials [31–40]. From the measurement, the grown PTLT crystal showed the suitability of the grown crystal for pharmaceutical applications.

4. Conclusion

In summary, p-Toluidinium L-Tartrate single crystal was grown at ambient temperature utilizing deionized water as a solvent. PXRD analysis confirmed the high crystalline nature of the compound which crystallizes in the *Triclinic* crystal system. The vibrations of functional groups were examined and enunciate the presence of the title compound. The UV-Vis-NIR spectrum shows the lower cut-off wavelength was found to be 315 nm. The extinction coefficient ($K = 1.9243 \times 10^{-6}$) and linear refractive index ($n_0 = 3.088$) were calculated using standard relation at 532 nm. The luminescence study confirms that the grown crystal can be utilized in the fabrication of violet LED and UV detector devices. The lower dielectric constant

Table 6
Comparison of antibacterial activity with other crystal materials.

Test organism	Crystal	Zone of inhibition (mm)	Reference
Bacillus cereus	CTSB	11	[31]
	LASN	14	[32]
	PTLT	18	Present work
Staphylococcus aureus	Co-DIC complex	21±0.77	[33]
	2APCS	22	[34]
	HTNN	16 ± 0.6	[35]
	CTSB	9	[31]
	NAKDP	15	[36]
	LYPB	13 ± 0.5	[37]
	PTLT	40	Present work
Shigella flexneri	ZTTC	22±0.7	[38]
	LASN	16	[32]
	PTLT	24	Present work
Pseudomonas aeruginosa	ZTTC	17±0.6	[38]
	Co-DIC complex	17±1.09	[33]
	HTNN	15 ± 0.2	[35]
	LASN	18	[32]
	γ-Glycine	28	[39]
Vibrio cholera	PTLT	35	Present work
	PCCH	17	[40]

and loss at higher frequency specifies that the sample is appropriate for optoelectronic device applications. Vickers microhardness study was used to confirm the soft material category and mechanical parameters were calculated. The frequency conversion efficiency of PTLT is comparable with KDP. The Z-Scan technique was examined and the crystal exhibits self-defocusing behaviour and reverse saturable absorption and hence it is useful for practical devices such as optical switching, optical limiter. The grown crystal has good antibacterial behaviour against tested foodborne bacterial strains and it can be used in biomedical applications.

Declaration of Competing Interest

There is no conflict of interest.

Acknowledgements

We are thankful to Prof. P. K. Das Department of Inorganic and Physical Chemistry, Indian Institute of Science, Bangalore for the SHG measurement. The authors P. S is thankful to UGC-NFHE [F1-17.1/2015-16/NFST-2015-17-ST-TAM-1335] and A. L would like to thank the UGC-RGNF [F1-17.1/2016-17/RGNF-2015-17-SC-TAM-21802] New Delhi, India, for the financial support.

References

[1] P. Karuppasamy, D. Joseph Daniel, H.J. Kim, M. Senthil Pandian, P. Ramasamy, Studies on semi-organic $(C_8H_{11}NO)_2[ZnCl_4]$ single crystal for nonlinear optical (NLO) applications, J. Cryst. Growth. 535 (2020) 125528.
[2] Z. Zang, All-optical switching in Sagnac loop mirror containing an ytterbium-doped fiber and fiber Bragg grating, Appl. Opt. 52 (2013) 5701.
[3] Z. Zang, Numerical analysis of optical bistability based on fiber Bragg grating cavity containing a high nonlinearity doped-fiber, Opt. Commun. 285 (2012) 521–526.
[4] Z. Zang, Y. Zhang, Analysis of optical switching in a Yb^{3+}-doped fiber Bragg grating by using self-phase modulation and cross-phase modulation, Appl. Opt. 51 (2012) 3424.
[5] Z.-G. Zang, Y.-J. Zhang, Low-switching power (<45 mW) optical bistability based on optical nonlinearity of ytterbium-doped fiber with a fiber Bragg grating pair, J. Mod. Opt. 59 (2012) 161–165.
[6] D.J. Daniel, P. Ramasamy, Studies on the nonlinear optical single crystal: ammonium d,l-tartrate $(C_4H_9NO_6)$, Mater. Res. Bull. 47 (2012) 708–713.
[7] C. Du, B. Teng, Z. Wang, J. Liu, X. Xu, G. Xu, K. Fu, J. Wang, Y. Liu, Z. Shao, Actively Q-switched intracavity second-harmonic generation of in BiB_3O_6 crystal, Opt. Laser Technol. 34 (2002) 343–346.
[8] S. Madhankumar, P. Muthuraja, M. Dhandapani, Hydrogen bond analysis of a third order nonlinear optical crystal, 2-amino-5-bromopyridinium benzilate, using structural and computational characterizations, J. Mol. Struct. 1203 (2020) 127419.
[9] S. Manivannan, Synthesis, crystal growth, structural and optical properties of an organic NLO material, J. Cryst. Growth. 262 (2004) 473–478.
[10] E.D. D'silva, G.K. Podagatlapalli, S. Venugopal Rao, S.M. Dharmaprakash, Study on third-order nonlinear optical properties of 4-methylsulfanyl chalcone derivatives using picosecond pulses, Mater. Res. Bull. 47 (2012) 3552–3557.
[11] P.S. Patil, M.S. Bannur, D.B. Badigannavar, S.M. Dharmaprakash, Study on nonlinear optical properties of 2, 4, 5-trimethoxy-4′-bromochalcone single crystal, Opt. Laser Technol. 55 (2014) 37–41.
[12] M.O. Senge, M. Fazekas, E.G.A. Notaras, W.J. Blau, M. Zawadzka, O.B. Locos, E.M. Ni Mhuircheartaigh, Nonlinear optical properties of porphyrins, Adv. Mater. 19 (2007) 2737–2774.
[13] M. Thangaraj, G. Ravi, T.C. Sabari Girisun, G. Vinitha, A. Loganathan, Ethylenediaminium di(4-nitrophenolate): a third order NLO material for optical limiting applications, Spectrochim. Acta Part A Mol. Biomol. Spectrosc. 138 (2015) 158–163.
[14] J.S. John, D. Sajan, T. Umadevi, K. Chaitanya, P. Sankar, R. Philip, Synthesis, crystal structure, vibrational spectral analysis and Z-scan studies of a new organic crystal N,N′dimethylurea ninhydrin: A scaled quantum mechanical force field study, Opt. Mater. (Amst). 48 (2015) 233–242.

[15] S. Madhankumar, P. Muthuraja, M. Dhandapani, Structural characterization, quantum chemical calculations and Hirshfeld surface analysis of a new third order harmonic organic crystal: 2-Amino-4-methylpyridinium benzilate, J. Mol. Struct. 1201 (2020) 127151.
[16] N. Sudharsana, V. Krishnakumar, R. Nagalakshmi, Synthesis, experimental and theoretical Studies of 8-hydroxyquinolinium 3,5-dinitrobenzoate single crystal, J. Cryst. Growth. 398 (2014) 45–57.
[17] G.J. Perpétuo, J. Janczak, Supramolecular architectures in crystals of melamine and aromatic carboxylic acids, J. Mol. Struct. 891 (2008) 429–436.
[18] T. Shanmugavadivu, K. Senthilkumar, M. Dhandapani, P. Muthuraja, S. Balachandar, M. Sethu Raman, Theoretical and experimental evaluation of a new organic proton transfer crystal aminoguanidinium p-nitrobenzoate monohydrate for optical limiting applications, J. Phys. Chem. Solids. 111 (2017) 82–94.
[19] S. Madhankumar, P. Muthuraja, M. Dhandapani, Physico-chemical characterization and computational studies of a new organic adduct 3-amino-2-chloropyridine: Benzilic acid, crystal for third order harmonic generation, J. Mol. Struct. 1203 (2020) 127415.
[20] K. Kamatchi, P. Umarani, T. Radhakrishnan, C. Ramachandra Raja, Investigation on organic-inorganic hybrid NLO crystal L-Valine potassium penta borate octa hydrate (LVPPB) for NLO applications, Optik (Stuttg) 172 (2018) 674–679.
[21] M.N. Bhat, S.M. Dharmaprakash, Growth of nonlinear optical γ-glycine crystals, J. Cryst. Growth. 236 (2002) 376–380.
[22] C. Janiak, A critical account on π–π stacking in metal complexes with aromatic nitrogen-containing ligands, J. Chem. Soc. Dalt. Trans. (2000) 3885–3896.
[23] G.R. Desiraju, C–H···O and other weak hydrogen bonds. From crystal engineering to virtual screening, Chem. Commun. (2005) 2995–3001.
[24] C.M.B. Pinilla, A. Brandelli, Antimicrobial activity of nanoliposomes co-encapsulating nisin and garlic extract against gram-positive and gram-negative bacteria in milk, Innov. Food Sci. Emerg. Technol. 36 (2016) 287–293.
[25] Karthik Kannan, Devi Radhika, Kishor Kumar Sadasivuni, Kakarla Raghava Reddy, Anjanapura V. Raghu, Nanostructured metal oxides and its hybrids for photocatalytic and biomedical applications, Adv. Colloid Interface Sci. 281 (2020) 102178.
[26] R. Aswini, S. Murugesan, Karthik Kannan, Bio-engineered TiO_2 nanoparticles using *Ledebouria revoluta* extract: Larvicidal, histopathological, antibacterial and anticancer activity, Intl. J. Environ. Anal. Chem. (2020), doi:10.1080/03067319.2020.1718668.
[27] K. Renuka, T.N.G. Row, B.R. Prasad, C.K. Subramanian, S. Bhattacharya, Hydrogen-bond-directed nonlinear-optical organic materials-evidence for the control of 2nd harmonic generation activities from the X-Ray crystal structures of the complexes of L-Tartaric acid with M-Anisidine and P-Toluidine, New J. Chem. 19 (1995) 83–89.
[28] S. Suresh, S. Reena Devi, B.M. Sornamurthy, M. Arivanandhan, R. Mohan Kumar, Growth, structural and optical studies of a novel nonlinear optical material: p-Toluidinium L-Tartrate, Optik (Stuttg) 185 (2019) 651–656.
[29] M. George, J. Balaji, D. Sajan, P. Dominic, R. Philip, G. Vinitha, Synthesis and third order optical nonlinearity studies of toluidine tartrate single crystal supported by photophysical characterization and vibrational spectral analysis, J. Photochem. Photobiol. A Chem. 393 (2020) 112413.
[30] J. Balaji, P. Srinivasan, S. Prabu, M. George, D. Sajan, Growth and dielectric studies of toluidine tartrate single crystals:A novel organic NLO material, J. Mol. Struct. 1207 (2020) 127750.
[31] J.Thomas Joseph Prakash, J.Martin Sam Gnanaraj, Growth and characterization of cadmium thiosemicarbazide bromide crystals for antibacterial and nonlinear optical applications, Spectrochim. Acta Part A Mol. Biomol. Spectrosc. 135 (2015) 25–30.
[32] M. Shanmuga Sundaram, V. Vijayalakshmi, P. Dhanasekaran, O.N. Balasundaram, S. Palaniswamy, Synthesis, crystallization, non linear optical and anti-bacterial activity of L-alanine sodium nitrate single crystals, J. Phys. Conf. Ser. 1172 (2019) 12072.
[33] F. Ashouri, A.R. Faraji, S. Molaeian, M.A. Fall, R.J. Butcher, The novel cobalt and manganese polymeric complex with the non-steroidal anti-inflammatory drug diclofenac: Synthesis, characterization and antibacterial studies, J. Mol. Struct. 1204 (2020) 127483.
[34] D. Sivavishnu, R. Srineevasan, J. Johnson, G. Vinitha, Data on in-vitro antibacterial activity and third order NLO property of 2-aminopyridine copper sulphate (2APCS), Chem. Data Collect. 25 (2020) 100319.
[35] V. Revathi, K. Karthik, Physico-chemical properties and antibacterial activity of Hexakis (Thiocarbamide) Nickel(II) nitrate single crystal, Chem. Data Collect. 21 (2019) 100229.
[36] B. Deepa, P. Philominathan, Enhanced NLO and antibacterial properties of nicotinic acid-doped KDP crystals: synthesis, growth and characterisation, Mater. Res. Innov. 21 (2017) 86–90.
[37] P. Yasotha, Growth, characterization, and antibacterial studies of L-Lysine single crystals added with potassium bromide, IOSR J. Appl. Phys. 9 (2017) 38–44.
[38] V. Revathi, K. Karthik, H. Mahdizadeh, Antibacterial activity and physico-chemical properties of metal-organic single crystal: Zinc (Tris) thiourea chloride, Chem. Data Collect. 24 (2019) 100279.
[39] V. Vijayalakshmi, P. Dhanasekaran, Growth and antimicrobial studies of γ-glycine crystal grown using $CuSO_4$, AIP Conf. Proc. 1953 (2018) 070004.
[40] V. Revathi, V. Rajendran, Investigation about nonlinear optics and antibacterial activity of pyrrolidine-2-carboxylic acid cadmium chloride hydrate single crystal, Optik (Stuttg) 154 (2018) 234–241.
[41] M.S. Dileep, H.M. Suresh Kumar, Effect of Co-60 gamma radiation on optical, dielectric and mechanical properties of strontium L-ascorbate hexahydrate NLO crystal, Radiat. Phys. Chem. 145 (2018) 104–110.
[42] Karthik Kannan, D. Radhika, S. Vijayalakshmi, Kishor Kumar Sadasivuni, Adaeze A. Ojiaku, Urvashi Verma, Facile fabrication of CuO nanoparticles via microwave-assisted method: photocatalytic, antimicrobial and anticancer enhancing performance, Int. J. Environ. Anal. Chem. (2020), doi:10.1080/03067319.2020.1733543.
[43] P. Surendran, A. Lakshmanan, S.S. Priya, K. Balakrishnan, P. Rameshkumar, T.A. Hegde, G. Vinitha, G. Ramalingam, A.A. Raj, Investigations on solid-state parameters of third-order nonlinear optical $Ni_{1-x}Zn_xFe_2O_4$ nanoparticles synthesized by microwave-assisted combustion method, Appl. Phys. A. 126 (2020) 257.
[44] J. Johnson, R. Srineevasan, D. Sivavishnu, In depth study on growth aspects and characteristic properties of semiorganic nonlinear optical crystal: 4-Dimethylaminopyridine copper chloride, Mater. Sci. Energy Technol. 2 (2019) 226–233.
[45] P. Prabu, R. Aarthi, R.Ramachandra Raja, Structural, spectral, thermal and nonlinear optical analysis of 4-fluoro salicylideneaniline crystal, Optik (Stuttg) 182 (2019) 458–463.
[46] R. Usha, N. Hema, V. Revathi Ambika, D. Shalini, D. Jayalakshmi, Synthesis, growth and characterization of nonlinear optical organic crystal: 4-Methoxy Anilinium 5-Sulfo Salicylate, Mater. Res. Innov. 23 (2019) 107–112.
[47] T. Shanmugavadivu, M. Dhandapani, Crystal structure, spectral, thermal, optical, laser damage, NLO study and quantum chemical calculations of a noncentrosymmetric crystal N, N′-diphenylguanidinium p-toluenesulphonate, J. Mol. Struct. 1179 (2019) 651–661.
[48] G. Saravana Kumar, P. Murugakoothan, Synthesis, spectral analysis, optical and thermal properties of new organic NLO crystal: N,N′-diphenylguanidinium nitrate (DPGN), Spectrochim. Acta Part A Mol. Biomol. Spectrosc. 131 (2014) 17–21.
[49] K. Pichan, S.P. Muthu, R. Perumalsamy, Crystal growth and characterization of third order nonlinear optical piperazinium bis(4-hydroxybenzenesulphonate) (P4HBS) single crystal, J. Cryst. Growth. 473 (2017) 39–54.
[50] S. Sakthy Priya, A. Alexandar, P. Surendran, A. Lakshmanan, P. Rameshkumar, P. Sagayaraj, Investigations on nucleation, HRXRD, optical, piezoelectric, polarizability and Z-scan analysis of l –arginine maleate dihydrate single crystals, Opt. Mater. (Amst). 66 (2017) 434–441.
[51] H.J.L. Hilary, P. Dhamodharan, P.C.J. Prabakar, A.C. Ferdinand, S. Thiyagaraj, N. Moorthy, Structural, optical, mechanical and dielectric property studies of adduct single crystal 2,4,6-trinitrobenzene-1,3-diol-2-methylimidazole: a spectroscopic and theoretical approach, Phys. B Condens. Matter. 567 (2019) 25–36.
[52] M. Rajkumar, P. Muthuraja, M. Dhandapani, A. Chandramohan, Synthesis, crystal structure, optical, thermal, mechanical, dielectric and DFT studies of 3, 5-dimethylprazole:1,3,5-benzene tricarboxylic acid molecular adduct crystal, Opt. Laser Technol. 124 (2020) 105970.
[53] E.M. Onitsch, Uber die Mikroharte der Metalle, Mikroscopia 2 (1947) 131–151.
[54] B.R. Lawn, D.B. Marshall, Hardness, toughness, and brittleness: an indentation analysis, J. Am. Ceram. Soc. 62 (1979) 347–350.

[55] B.R. Lawn, A.G. Evans, A model for crack initiation in elastic/plastic indentation fields, J. Mater. Sci. 12 (1977) 2195–2199.
[56] W.A. Wooster, Physical properties and atomic arrangements in crystals, Reports Prog. Phys. 16 (1953) 302.
[57] K. Senthil, A. Senthil, K. Elangovan, Crystal structure, growth and physiochemical properties of nonlinear optical single crystal: Bis(cyclohexylammonium) dioxalate hydrate, J. Mol. Struct. 1209 (2020) 127926.
[58] M. Sheik-Bahae, A.A. Said, T.-H. Wei, D.J. Hagan, E.W. Van Stryland, Sensitive measurement of optical nonlinearities using a single beam, IEEE J. Quantum Electron. 26 (1990) 760–769.
[59] T. Ashok Hegde, A. Dutta, G. Vinitha, $\chi^{(3)}$ measurement and optical limiting behaviour of novel semi-organic cadmium mercury thiocyanate crystal by Z-scan technique, Appl. Phys. A. 124 (2018) 808.
[60] T.A. Hegde, A. Dutta, T.C. Sabari Girisun, M. Abith, G. Vinitha, Intensity tunable optical limiting behavior of an organometallic cesium hydrogen tartrate single crystal, J. Mater. Sci. Mater. Electron. 30 (2019) 18885–18896.
[61] P. Surendran, A. Lakshmanan, G. Vinitha, G. Ramalingam, P. Rameshkumar, Facile preparation of high fluorescent carbon quantum dots from orange waste peels for nonlinear optical applications, Luminescence 35 (2020) 196–202.
[62] S. Yuvaraj, N. Manikandan, G. Vinitha, Influence of copper ions on structural and non-linear optical properties in manganese ferrite nanomaterials, Opt. Mater (Amst). 73 (2017) 428–436.
[63] P. Karuppasamy, M. Senthil Pandian, P. Ramasamy, S. Verma, Crystal growth, structural, optical, thermal, mechanical, laser damage threshold and electrical properties of triphenylphosphine oxide 4-nitrophenol (TP4N) single crystals for nonlinear optical applications, Opt. Mater. (Amst). 79 (2018) 152–171.
[64] A. Arunkumar, P. Ramasamy, Bulk single crystals of ammonium acid phthalate grown by the Sankaranarayanan–Ramasamy method for optical limiting applications, J. Cryst. Growth. 401 (2014) 195–199.
[65] S.E. Allen Moses, S. Tamilselvan, S.M. Ravi Kumar, G. Vinitha, T.A. Hegde, M. Vimalan, S. Varalakshmi, S. Sivaraj, Synthesis, growth and physicochemical properties of new organic nonlinear optical crystal l-threoninium tartrate (LTT) for frequency conversion, Mater. Sci. Energy Technol. 2 (2019) 565–574.
[66] M.Krishna Kumar, S. Sudhahar, P. Pandi, G. Bhagavannarayana, R.Mohan Kumar, Studies of the structural and third-order nonlinear optical properties of solution grown 4-hydroxy-3-methoxy-4′-N′-methylstilbazolium tosylate monohydrate crystals, Opt. Mater. (Amst). 36 (2014) 988–995.
[67] S.E. Allen Moses, S. Tamilselvan, S.M. Ravi Kumar, G. Vinitha, T.A. Hegde, G.J. Shanmuga Sundar, M. Vimalan, S. Sivaraj, Crystal structure, spectroscopic, thermal, mechanical, linear optical, second order and third order nonlinear optical properties of semiorganic crystal: l-threoninium phosphate (LTP), J. Mater. Sci. Mater. Electron. 30 (2019) 9003–9014.
[68] Karthik Kannan, D. Radhika, Maria P. Nikolova, V. Andal, Kishor Kumar Sadasivuni, L. Sivarama Krishna, Facile microwave-assisted synthesis of metal oxide CdO-CuO nanocomposite: photocatalytic and antimicrobial enhancing properties, Optik 218 (2020) 165112.
[69] A. Lakshmanan, P. Surendran, S. SakthyPriya, K. Balakrishnan, T.A. Hegde, G. Vinitha, G. Ramalingam, B. Ravindran, S.W. Chang, M.S. Elshikh, A.H. Mahmoud, D.A. Al Farraj, P. Rameshkumar, Effect of fuel content on nonlinear optical and antibacterial activities of Zn/Cu/Al_2O_4 nanoparticles prepared by microwave-assisted combustion method, J. King Saud Univ. - Sci. 32 (2020) 1382–1389.
[70] M. Tamil Elakkiya, K. Anitha, Structural investigation, spectral characterization, thermal and antibacterial activity on a organic crystal: 2-Aminopyrazin-1-ium3-carbaoxypicolinate, Mater. Lett. 235 (2019) 202–206.
[71] M. Tamil Elakkiya, S. PremKumar, M. Sathiyendran, P. Suresh, V. Shanmugaiah, K. Anitha, Structural, spectral, computational, thermal and antibacterial studies on a co-crystal: 2-Aminopyrazine phthalic acid, J. Mol. Struct. 1173 (2018) 635–646.
[72] G.B. Dani RK, P.R. Srivastava M, Y.R. Gondwal M, Synthesis, characterization, single crystal structural studies, antibacterial activity and DFT investigations of 2-Chloro-5-Ethoxy-3,6-Bis(Methylamino)-1,4-Benzoquinone, Pharm. Anal. Acta 6 (2015) 1000418.
[73] P. Surendran, A. Lakshmanan, S.S. Priya, K. Balakrishnan, P. Rameshkumar, K. Kannan, P. Geetha, T.A. Hegde, G. Vinitha, Bioinspired fluorescence carbon quantum dots extracted from natural honey: efficient material for photonic and antibacterial applications, Nano-Struct. Nano-Obj. 24 (2020) 00589.